Chinese Journal of Aeronautics, 2013,26(3): 741–750

Chinese Society of Aeronautics and Astronautics
& Beihang University

Chinese Journal of Aeronautics

cja@buaa.edu.cn
www.sciencedirect.com

Adaptive block dynamic surface control for integrated missile guidance and autopilot

Hou Mingzhe *, Liang Xiaoling, Duan Guangren

Center for Control Theory and Guidance Technology, Harbin Institute of Technology, Harbin 150001, China

Received 10 March 2012; revised 5 May 2012; accepted 18 December 2012
Available online 30 April 2013

KEYWORDS

Adaptive control;
Block dynamic surface control;
Integrated guidance and autopilot;
Missile control;
Nonlinear control

Abstract A novel integrated guidance and autopilot design method is proposed for homing missiles based on the adaptive block dynamic surface control approach. The fully integrated guidance and autopilot model is established by combining the nonlinear missile dynamics with the nonlinear dynamics describing the pursuit situation of a missile and a target in the three-dimensional space. The integrated guidance and autopilot design problem is further converted to a state regulation problem of a time-varying nonlinear system with matched and unmatched uncertainties. A new and simple adaptive block dynamic surface control algorithm is proposed to address such a state regulation problem. The stability of the closed-loop system is proven based on the Lyapunov theory. The six degrees of freedom (6DOF) nonlinear numerical simulation results show that the proposed integrated guidance and autopilot algorithm can ensure the accuracy of target interception and the robust stability of the closed-loop system with respect to the uncertainties in the missile dynamics.

1. Introduction

The traditional design method of the missile guidance and autopilot system is to design each subsystem separately and then integrate them. In order to achieve the desired overall system performance, modifications are generally inevitably required to each subsystem. Hence such a design approach usually leads to excessive design iterations and high costs. What's more, it is argued that this approach may not fully exploit the synergistic relationships between these two interacting subsystems. As a result, the performance of the overall system may be constrained.[1,2]

To overcome this problem, a new design method called integrated guidance and autopilot was proposed. Integrated guidance and autopilot directly generates the fin deflection commands according to the states of the missile and the target relative to the missile to drive the missile to intercept the target.[1] In the integrated guidance and autopilot system, there is no separation between guidance and autopilot.[2] Therefore, the synergistic relationships between the coupled subsystems can be fully exploited to optimize the performance of the overall system. Due to this reason, integrated guidance and autopilot has received more and more attention recently.[1–10]

However, most of the existing relevant literature is on the three-channel independent design idea and is focused on the

* Corresponding author. Tel.: +86 451 86418034.
E-mail addresses: hithyt@gmail.com (M. Hou), lxl_dmu2008@126.com (X. Liang), g.r.duan@hit.edu.cn (G. Duan).

Peer review under responsibility of Editorial Committe of CJA.

ELSEVIER Production and hosting by Elsevier

1000-9361
http://dx.doi.org/10.1016/j.cja.2013.04.035

Nomenclature

α	angle of attack (rad)
β	angle of sideslip (rad)
γ	roll angle (rad)
ψ	yaw angle (rad)
ϑ	pitch angle (rad)
θ	flight path angle (rad)
ψ_V	heading angle (rad)
ω_x, ω_y, ω_z	body-axis roll, yaw and pitch rates (rad/s)
δ_x, δ_y, δ_z	aileron, Rudder and elevator deflections (rad/s)
V	velocity of the missile (m/s)
m	mass of the missile (kg)
P	thrust force (N)
ρ	air density (kg/m^3)
$q = 0.5\rho V^2$	dynamic pressure (Pa)
J_x, J_y, J_z	roll, yaw and pitch moments of inertia (kg·m^2)
X,Y,Z	drag, lift and side forces (N)
S	reference area (m^2)
L	reference length (m)
ε	elevation angle of the line-of-sight (rad)
η	azimuth angle of the line-of-sight (rad)
R	missile–target range (m)
r	missile–target range in horizon plane (m)
c_{x0}	zero-lift drag coefficient
c_x^α, c_x^β	partial derivatives of drag force coefficient with respect to α and β
$c_x^{\delta_x}, c_x^{\delta_y}, c_x^{\delta_z}$	partial derivatives of drag force coefficient with respect to δ_x, δ_y and δ_z
$c_x^{\alpha\beta}$	second partial derivative of drag force coefficient with respect to α and β
$c_y^\alpha, c_y^\beta, c_y^{\delta_z}$	partial derivatives of lift force coefficient with respect to α, β and δ_z
$c_z^\alpha, c_z^\beta, c_z^{\delta_y}$	partial derivatives of side force coefficient with respect to α, β and δ_y
$m_x^{\delta_x}, m_x^\alpha, m_x^\beta$	partial derivatives of rolling moment coefficient with respect to δ_x, α and β
$m_y^\beta, m_y^{\delta_y}$	partial derivatives of yawing moment coefficient with respect to β and δ_y
$m_z^\alpha, m_z^{\delta_z}$	partial derivatives of pitching moment coefficient with respect to α and δ_z

integrated guidance and autopilot design when the missile and the target only move in the same plane. Only a few of them consider the coupled relationships among different channels of the missile dynamics, which in fact can also be exploited to improve the performance of the overall system. In the recent literature, some control methods like feedback linearization method,[1] nonlinear optimal control method including state-dependent Riccati equation (SDRE) method[2,8] and θ–D method,[9] etc., have been applied to the integrated guidance and autopilot framework where the full nonlinear missile dynamics is used. But these methods all involve complicated numerical computations. For example, in the feedback linearization method,[1] complicated numerical computations are required to transform the nonlinear system into a linear system, and then the linear control method is used; in the nonlinear optimal control method,[2,8,9] it is needed to solve the Hamilton–Jacobi–Bellman (HJB) equation on-line, hence complicated numerical calculations are also unavoidable. What is more, these methods cannot ensure the robustness of the closed-loop system. Therefore, it is necessary and interesting to develop simple and effective fully integrated guidance and autopilot algorithms with good performance and stability robustness.

In the current paper, an integrated guidance and autopilot algorithm is proposed for a kind of homing missiles at the stage of diving to attack, that is, the passive homing phase. This kind of missiles is used to attack ground targets and adopt the skid-to-turn (STT) technology. First of all, the integrated guidance and autopilot model is established by combining the nonlinear missile dynamics with the nonlinear dynamics describing the pursuit situation of a missile and a target in the three-dimensional space. As a result, the integrated guidance and autopilot design problem is converted to a state regulation problem of a time-varying nonlinear system with matched and unmatched uncertainties. Fortunately, this model satisfies the so-called block low-triangular structure, which makes it possible to design the control algorithm utilizing the block backstepping methodology.[11] However, the block backstepping methodology suffers from the problem of "explosion of complexity" arising from the repeated differentiations of the virtual controls. As a consequence, the complexity of the control algorithm grows drastically as the order of the system increases. To avoid such a problem, a block dynamic surface control approach is proposed in this paper by introducing a set of first-order filters at each step of the traditional block backstepping approach.

The proposed adaptive block dynamic surface control approach can be viewed as an extension of the traditional dynamic surface control approach.[10,12–14] The stability analysis of the closed-loop system is also given based on the Lyapunov theory. The six degrees of freedom (6DOF) nonlinear numerical simulation results show that the proposed feedback controller can ensure the accuracy of target interception and the robust stability of the closed-loop system with respect to the inevitable uncertainties in the missile dynamics.

2. Problem formulation

In this section, the integrated model of the missile guidance and autopilot system is firstly established. Then, the control design objective of this paper is presented.

2.1. Model derivation

The nonlinear missile dynamics with uncertainties is described by[15,16]

$$\begin{cases} \dot{\boldsymbol{x}}_1 = \boldsymbol{f}_1(\boldsymbol{x}_1) + \boldsymbol{g}_1(\vartheta, \boldsymbol{x}_1)\boldsymbol{x}_2 + \boldsymbol{d}_1(t) \\ \dot{\boldsymbol{x}}_2 = \boldsymbol{f}_2(\boldsymbol{x}_1, \boldsymbol{x}_2) + \boldsymbol{g}_2(t)\boldsymbol{u} + \boldsymbol{d}_2(t) \end{cases} \tag{1}$$

with

$$\boldsymbol{x}_1 = \begin{bmatrix} \gamma \\ \beta \\ \alpha \end{bmatrix}, \quad \boldsymbol{x}_2 = \begin{bmatrix} \omega_x \\ \omega_y \\ \omega_z \end{bmatrix}, \quad \boldsymbol{u} = \begin{bmatrix} \delta_x \\ \delta_y \\ \delta_z \end{bmatrix}$$

$$\boldsymbol{f}_1(\boldsymbol{x}_1)=\begin{bmatrix}0\\ \frac{1}{mV}\left(qSc_z^{\beta}\beta-P\cos\alpha\sin\beta\right)\\ -\frac{1}{mV\cos\beta}\left(P\sin\alpha+qSc_y^{\alpha}\alpha\right)\end{bmatrix}$$

$$\boldsymbol{g}_1(\vartheta,\boldsymbol{x}_1)=\begin{bmatrix}1 & -\tan\vartheta\cos\gamma & \tan\vartheta\sin\gamma\\ \sin\alpha & \cos\alpha & 0\\ -\tan\beta\cos\alpha & \sin\alpha\tan\beta & 1\end{bmatrix}$$

$$\boldsymbol{f}_2(\boldsymbol{x}_1,\boldsymbol{x}_2)=\begin{bmatrix}\frac{J_z-J_y}{J_x}\omega_y\omega_z\\ \frac{1}{J_y}qSLm_y^{\beta}\beta+\frac{J_x-J_z}{J_y}\omega_x\omega_z\\ \frac{1}{J_z}qSLm_z^{\alpha}\alpha+\frac{J_y-J_x}{J_z}\omega_x\omega_y\end{bmatrix}$$

$$\boldsymbol{g}_2(t)=\begin{bmatrix}\frac{1}{J_x}qSLm_x^{\delta_x} & 0 & 0\\ 0 & \frac{1}{J_y}qSLm_y^{\delta_y} & 0\\ 0 & 0 & \frac{1}{J_z}qSLm_z^{\delta_z}\end{bmatrix}$$

where the dynamics of the pitching angle is given by [17]

$$\dot{\vartheta}=\omega_y\sin\gamma+\omega_z\cos\gamma \tag{2}$$

and $\boldsymbol{d}_1(t)$ and $\boldsymbol{d}_2(t)$ are the uncertain terms cased by the uncertainties of the missile-related parameters, for example, the aerodynamic coefficients, etc.

On the other hand, as shown in Fig. 1, the pursuit situation of a missile and a target in the three-dimensional space can be described by the following nonlinear differential equations[18,19]:

$$\begin{bmatrix}\ddot{R}-R\dot{\varepsilon}^2-R\dot{\eta}^2\cos^2\varepsilon\\ 2\dot{R}\dot{\varepsilon}+R\ddot{\varepsilon}+r\dot{\eta}^2\sin\varepsilon\\ -2\dot{R}\dot{\eta}\cos\varepsilon-r\ddot{\eta}+2R\dot{\eta}\dot{\varepsilon}\sin\varepsilon\end{bmatrix}=\begin{bmatrix}a_{t4x}\\ a_{t4y}\\ a_{t4z}\end{bmatrix}-\begin{bmatrix}a_{4x}\\ a_{4y}\\ -a_{4z}\end{bmatrix} \tag{3}$$

where $\boldsymbol{a}_{t4}=[a_{t4x}\quad a_{t4y}\quad a_{t4z}]^{\mathrm{T}}$ is the acceleration vector of the target in the line-of-sight (LOS) coordinate system, $\boldsymbol{a}_4=[a_{4x}\quad a_{4y}\quad a_{4z}]^{\mathrm{T}}$ the acceleration vector of the missile in the LOS coordinate system. From Eq. (3), one has

$$\begin{bmatrix}\ddot{\eta}\\ \ddot{\varepsilon}\end{bmatrix}=-\begin{bmatrix}\frac{2\dot{R}\dot{\eta}\cos\varepsilon}{r}-\frac{2R\dot{\eta}\dot{\varepsilon}}{r}\sin\varepsilon\\ \frac{2\dot{R}\dot{\varepsilon}}{R}+\frac{\dot{\eta}^2 r\sin\varepsilon}{R}\end{bmatrix}+\begin{bmatrix}\frac{1}{r} & 0\\ 0 & -\frac{1}{R}\end{bmatrix}\begin{bmatrix}a_{4z}\\ a_{4y}\end{bmatrix}+\begin{bmatrix}-\frac{a_{t4z}}{r}\\ \frac{a_{t4y}}{R}\end{bmatrix} \tag{4}$$

The acceleration components of the missile along the z- and y-axes of the missile velocity coordinate system are given by[17]

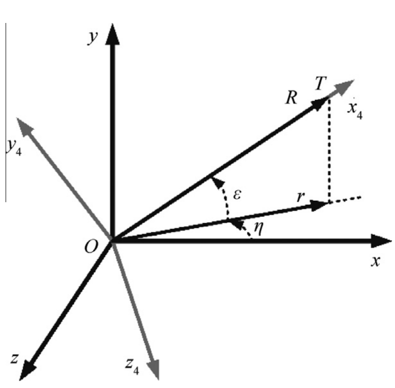

Fig. 1 Pursuit geometry in three-dimensional space.

$$\begin{bmatrix}a_{3z}\\ a_{3y}\end{bmatrix}=\frac{1}{m}\begin{bmatrix}-P\cos\alpha\sin\beta+Z\\ P\sin\alpha+Y\end{bmatrix} \tag{5}$$

where Y and Z are given by

$$\begin{cases}Z=qSc_z^{\beta}\beta+d_Z\\ Y=qSc_y^{\alpha}\alpha+d_Y\end{cases} \tag{6}$$

where d_Z and d_Y are, respectively, the side force and lift force caused by the other factors, for example, the control surfaces, etc. Each of these two terms is much smaller than its left term in the right side of the above equations. So d_Z and d_Y can be considered as uncertain terms. When α and β are small enough, we have $\sin\alpha\approx\alpha$, $\sin\beta\approx\beta$ and $\cos\alpha\approx 1$. Then from Eq. (6), one can obtain

$$\begin{bmatrix}a_{3z}\\ a_{3y}\end{bmatrix}=\begin{bmatrix}\frac{qSc_z^{\beta}-P}{m} & 0\\ 0 & \frac{qSc_y^{\alpha}+P}{m}\end{bmatrix}\begin{bmatrix}\beta\\ \alpha\end{bmatrix}+\begin{bmatrix}d_{3z}\\ d_{3y}\end{bmatrix} \tag{7}$$

where $[d_{3z}\quad d_{3y}]^{\mathrm{T}}$ represents the approximation errors between $[a_{3z}\quad a_{3y}]^{\mathrm{T}}$ and the first term on the right side of Eq. (7).

If the missile flies heading to the target at initial time (this can be satisfied in many cases), then the missile velocity coordinate system approximately coincides with the LOS coordinate system. As a result, one has

$$\begin{bmatrix}a_{4z}\\ a_{4y}\end{bmatrix}=\begin{bmatrix}a_{3z}\\ a_{3y}\end{bmatrix}+\begin{bmatrix}d_{4z}\\ d_{4y}\end{bmatrix} \tag{8}$$

where $[d_{4z}\quad d_{4y}]^{\mathrm{T}}$ represents the approximation errors between $[a_{4z}\quad a_{4y}]^{\mathrm{T}}$ and $[a_{3z}\quad a_{3y}]^{\mathrm{T}}$.

Define

$$x_{01}=\dot{\eta},\quad x_{02}=\dot{\varepsilon}$$

and

$$\boldsymbol{x}_0=\begin{bmatrix}x_{01}\\ x_{02}\end{bmatrix},\quad \boldsymbol{x}_1^{\#}=\begin{bmatrix}\beta\\ \alpha\end{bmatrix}$$

then combining Eqs. (7) and (8) with Eq. (4), we have

$$\dot{\boldsymbol{x}}_0=\boldsymbol{f}_0(\boldsymbol{x}_0)+\boldsymbol{g}_0(t)\boldsymbol{x}_1^{\#}+\boldsymbol{d}_0(t) \tag{9}$$

where

$$\boldsymbol{f}_0(\boldsymbol{x}_0)=-\begin{bmatrix}\frac{2\dot{R}x_{01}}{r}\cos\varepsilon-\frac{2Rx_{01}x_{02}}{r}\sin\varepsilon\\ \frac{2\dot{R}x_{02}}{R}+\frac{x_{01}^2 r}{R}\sin\varepsilon\end{bmatrix}$$

$$\boldsymbol{g}_0(t)=\begin{bmatrix}\frac{qSc_z^{\beta}-P}{mr} & 0\\ 0 & -\frac{qSc_y^{\alpha}+P}{mR}\end{bmatrix}$$

and $\boldsymbol{d}_0(t)$ represents the uncertainty.

According to the above analysis, the integrated model of the guidance and autopilot system for homing missiles can be written as

$$\begin{cases}\dot{\boldsymbol{x}}_0=\boldsymbol{f}_0(\boldsymbol{x}_0)+\boldsymbol{g}_0(t)\boldsymbol{x}_1^{\#}+\boldsymbol{d}_0(t)\\ \dot{\boldsymbol{x}}_1=\boldsymbol{f}_1(\boldsymbol{x}_1)+\boldsymbol{g}_1(\vartheta,\boldsymbol{x}_1)\boldsymbol{x}_2+\boldsymbol{d}_1(t)\\ \dot{\boldsymbol{x}}_2=\boldsymbol{f}_2(\boldsymbol{x}_1,\boldsymbol{x}_2)+\boldsymbol{g}_2(t)\boldsymbol{u}+\boldsymbol{d}_2(t)\end{cases} \tag{10}$$

In this paper, the uncertainties $\boldsymbol{d}_0(t)$, $\boldsymbol{d}_1(t)$ and $\boldsymbol{d}_2(t)$ are assumed to satisfy Assumption 1.

Assumption 1. There exist a set of unknown constants ρ_i $(i=0,1,2)$ such that

$$\|\boldsymbol{d}_i(t)\| \leqslant \rho_i$$

System (10) is a time-varying nonlinear system with unmatched uncertainties $d_0(t)$ and $d_1(t)$, and matched uncertainty $\boldsymbol{d}_2(t)$. Here it is assumed that these uncertainties are all norm-bounded, but the bounds are unknown.

It is noted that when the missile is close to the target enough, the seeker will operate in its dead zone; as a result, the integrated guidance and autopilot system will not work anymore. Hence, we just need to consider the situation when $r \geqslant r_f$, or equivalently, $R \geqslant R_f$, where r_f and R_f are two positive numbers related to the dead zone of the seeker. In this case, $\boldsymbol{g}_0(t)$ is well defined since $m > 0$. Furthermore, we assume that $\boldsymbol{g}_0(t)$ satisfies Assumption 2 below.

Assumption 2. The elements of $\boldsymbol{g}_0(t)$ and $\boldsymbol{g}_0^{-1}(t)$ together with their derivatives are all bounded.

This assumption will be used in the stability analysis of the closed-loop system.

Simple computation yields

$$\det(\boldsymbol{g}_1(\vartheta, \boldsymbol{x}_1)) = \cos\alpha + (\cos\gamma\sin\alpha + \tan\beta\sin\gamma)\tan\vartheta$$

hence Lemma 1 is immediate.

Lemma 1. There exist three positive constants

$$0 < \vartheta_m < \frac{\pi}{2}, \quad 0 < \alpha_m < \frac{\pi}{2}, \quad 0 < \beta_m < \frac{\pi}{2}$$

such that $\boldsymbol{g}_1$ is invertible for arbitrary variable γ and

$$(\alpha, \beta, \vartheta) \in \{(\alpha, \beta, \vartheta) : |\alpha| \leqslant \alpha_m, |\beta| \leqslant \beta_m, |\vartheta| \leqslant \vartheta_m\}$$

According to Lemma 1, we give Assumption 3 which is useful in the sequential control design and analysis process.

Assumption 3. Throughout the engagement, the relationship

$$(\alpha, \beta, \vartheta) \in B_2 = \{(\alpha, \beta, \vartheta) : |\alpha| \leqslant \alpha_m, |\beta| \leqslant \beta_m, |\vartheta| \leqslant \vartheta_m\}$$

always holds.

Assumption 3 is mainly used to ensure that $\boldsymbol{g}_1$ is invertible, since the inverse of $\boldsymbol{g}_1$ will be used in the proposed integrated guidance and autopilot algorithm. In most cases, this assumption can be satisfied. However, whether this assumption is really satisfied can only be verified when α_m, β_m and ϑ_m are obtained from the simulation results.

2.2. Design objective

In this paper, the main guidelines for the design of the integrated guidance and autopilot algorithm are given as follows:

(1) To intercept the maneuvering targets with small miss distance.
(2) To maintain the change of the roll angle near zero throughout the engagement.
(3) To stabilize the states of the missile.
(4) To be robust with respect to the inevitable uncertainties existing in the missile dynamics. That is to say, the above three guidelines should also be satisfied when there exist uncertainties in the missile dynamics.

According to the parallel approaching method,[20] to acquire a zero miss-distance, the LOS direction should be kept constant ultimately. Hence, to satisfy the first guideline, $\dot{\eta}$ and $\dot{\varepsilon}$ should be driven to zero as much as possible. The second guideline can be satisfied by maintaining the roll angle γ near zero throughout the engagement if the initial roll angle is set as zero. And the third guideline requires that the states of the missile should be kept bounded (Strictly speaking, each one of the states should be kept in a reasonable bound, but this problem is too difficult to be solved at present).

Therefore, the integrated guidance and autopilot algorithm design problem can be viewed as the state regulation problem of the uncertain nonlinear system (10), that is, to propose an appropriate control algorithm for system (10) not only to drive its partial states x_{01} (i.e., $\dot{\eta}$), x_{02} (i.e., $\dot{\varepsilon}$) and x_{11} (i.e., γ) (x_{ij} refers to the jth element of the state vector $\boldsymbol{x}_i$) to zero as much as possible, but also to ensure that all the states of the closed-loop system are kept bounded.

3. Control design and stability analysis

In this section, an adaptive block dynamic surface control algorithm is developed for the uncertain nonlinear system (10) which can drive the states x_{01}, x_{02} and x_{11} into a neighborhood of zero, and keep the other states bounded simultaneously.

3.1. Control algorithm

System (10) is a time-varying nonlinear system with matched and unmatched uncertainties. For such a kind of nonlinear systems, the most natural control method is the block backstepping approach since the system satisfies the so-called block low-triangular structure. But the traditional block backstepping methodology suffers from the problem of "explosion of complexity" arising from the repeated differentiations of the virtual controls. To avoid this problem, an adaptive block dynamic surface controller is given as follows:

$$\begin{cases} \boldsymbol{s}_0 = \boldsymbol{x}_0 \\ \boldsymbol{x}_{1d}^{\#} = -\boldsymbol{g}_0^{-1}(t)(\mu_0\boldsymbol{s}_0 + \boldsymbol{f}_0(\boldsymbol{x}_0)) + \boldsymbol{k}_0\boldsymbol{s}_0 \\ \boldsymbol{\tau}_1\dot{\boldsymbol{x}}_{1c}^{\#} + \boldsymbol{x}_{1c}^{\#} = \boldsymbol{x}_{1d}^{\#} \\ \boldsymbol{s}_1 = \boldsymbol{x}_1 - \begin{bmatrix} 0 \\ \boldsymbol{x}_{1c}^{\#} \end{bmatrix} \\ \boldsymbol{x}_{2d} = \boldsymbol{g}_1^{-1}(\vartheta, \boldsymbol{x}_1)\left(-\mu_1\boldsymbol{s}_1 - \boldsymbol{k}_1\boldsymbol{s}_1 - \boldsymbol{f}_1(\boldsymbol{x}_1) + \begin{bmatrix} 0 \\ \dot{\boldsymbol{x}}_{1c}^{\#} \end{bmatrix}\right) \\ \boldsymbol{\tau}_2\dot{\boldsymbol{x}}_{2c} + \boldsymbol{x}_{2c} = \boldsymbol{x}_{2d} \\ \boldsymbol{s}_2 = \boldsymbol{x}_2 - \boldsymbol{x}_{2c} \\ \boldsymbol{u} = \boldsymbol{g}_2^{-1}(t)(-\boldsymbol{k}_2\boldsymbol{s}_2 - \mu_2\boldsymbol{s}_2 - \boldsymbol{f}_2(\boldsymbol{x}_1, \boldsymbol{x}_2) + \dot{\boldsymbol{x}}_{2c}) \end{cases} \tag{11}$$

where $\boldsymbol{s}_0$, $\boldsymbol{s}_1$ and $\boldsymbol{s}_2$ are the dynamic surface vectors; $\boldsymbol{k}_0$ = diag(k_{01}, k_{02}), $\boldsymbol{k}_1$ = diag(k_{11}, k_{12}, k_{13}) and $\boldsymbol{k}_2$ = diag(k_{21}, k_{22}, k_{23}) denotes the dynamic surface gain matrices, whose elements are called the dynamic surface gains; the control algorithm includes three steps starting from $\boldsymbol{s}_0$, $\boldsymbol{s}_1$ and $\boldsymbol{s}_2$, respectively; $\boldsymbol{x}_{1d}^{\#}$ and $\boldsymbol{x}_{2d}$ (where the index "d" means "desired") are the virtual control vectors obtained from the first and the second steps; $\boldsymbol{x}_{1c}^{\#}$ and $\boldsymbol{x}_{2c}$ (where the index "c" means "command") are the command inputs of the second step and the third step, which are obtained by letting $\boldsymbol{x}_{1d}^{\#}$ and $\boldsymbol{x}_{2d}$,

respectively, pass through a set of low pass filters (i.e., the third and the sixth equations of the control algorithm (11)); $\boldsymbol{\tau}_1 = \mathrm{diag}(\tau_{11}, \tau_{12})$ and $\boldsymbol{\tau}_2 = \mathrm{diag}(\tau_{21}, \tau_{22}, \tau_{23})$ denote the filter time constant matrices, whose elements are called the filter time constants; μ_i is the estimate of ρ_i and satisfies the following updating law

$$\dot{\mu}_i = \lambda_i\left(\boldsymbol{s}_i^{\mathrm{T}}\boldsymbol{s}_i - \sigma_i\mu_i\right) \tag{12}$$

where λ_i and σ_i are positive design parameters.

Remark 1. If let $\boldsymbol{\tau}_1 = \boldsymbol{0}$ and $\boldsymbol{\tau}_2 = \boldsymbol{0}$, then $\boldsymbol{x}_{1c}^{\#} = \boldsymbol{x}_{1d}^{\#}$ and $\boldsymbol{x}_{2c} = x_{2d}$; as a result, the control algorithm (11) becomes the traditional block backstepping control approach. In this case, it is necessary to compute the differentiations of the virtual controls repeatedly, which will result in a complex control algorithm. In our algorithm, by introducing two sets of filters, the repeated differentiations of the virtual controls are avoided. In addition, it is noted that the derivatives of the command inputs can be obtained by simple algebraic manipulations as follows:

$$\dot{\boldsymbol{x}}_{1c}^{\#} = \boldsymbol{\tau}_1^{-1}\left(\boldsymbol{x}_{1d}^{\#} - \boldsymbol{x}_{1c}^{\#}\right) \tag{13}$$

$$\dot{\boldsymbol{x}}_{2c} = \boldsymbol{\tau}_2^{-1}(\boldsymbol{x}_{2d} - \boldsymbol{x}_{2c}) \tag{14}$$

Remark 2. Compared to the existing integrated and autopilot algorithms based on the feedback linearization or the nonlinear optimal control method, the proposed integrated guidance and autopilot algorithm (11) is very simple and analytic, avoiding complicated computations.

3.2. Stability analysis

For simplification, a function $\boldsymbol{f}(\cdot)$ will be denoted by $\boldsymbol{f}$ in the following process.

Define the boundary layer error vectors as

$$\boldsymbol{y}_1 = \boldsymbol{x}_{1c}^{\#} - \boldsymbol{x}_{1d}^{\#} \tag{15}$$

$$\boldsymbol{y}_2 = \boldsymbol{x}_{2c} - \boldsymbol{x}_{2d} \tag{16}$$

and the estimate error vectors as

$$e_i = \rho_i - \mu_i \quad (i = 0, 1, 2) \tag{17}$$

then we have

$$\dot{\boldsymbol{y}}_1 = -\boldsymbol{\tau}_1^{-1}\boldsymbol{y}_1 - \dot{\boldsymbol{x}}_{1d}^{\#} \tag{18}$$

$$\dot{\boldsymbol{y}}_2 = -\boldsymbol{\tau}_2^{-1}\boldsymbol{y}_2 - \dot{\boldsymbol{x}}_{2d} \tag{19}$$

and

$$\dot{e}_i = -\dot{\mu}_i = -\lambda_i\left(\boldsymbol{s}_i^{\mathrm{T}}\boldsymbol{s}_i - \sigma_i\mu_i\right) \quad (i = 0, 1, 2) \tag{20}$$

According to Eqs. (11), (15) and (16), we have

$$\boldsymbol{x}_0 = \boldsymbol{s}_0 \tag{21}$$

$$\boldsymbol{x}_1 = \boldsymbol{s}_1 + \begin{bmatrix} 0 & \left(\boldsymbol{x}_{1c}^{\#}\right)^{\mathrm{T}} \end{bmatrix}^{\mathrm{T}} = \boldsymbol{s}_1 + \begin{bmatrix} 0 & \left(\boldsymbol{y}_1 + \boldsymbol{x}_{1d}^{\#}\right)^{\mathrm{T}} \end{bmatrix}^{\mathrm{T}} \tag{22}$$

and

$$\boldsymbol{x}_2 = \boldsymbol{s}_2 + \boldsymbol{x}_{2c} = \boldsymbol{s}_2 + \boldsymbol{y}_2 + \boldsymbol{x}_{2d} \tag{23}$$

Define

$$\boldsymbol{s}_1^{\#} = \boldsymbol{x}_1^{\#} - \boldsymbol{x}_{1c}^{\#} \tag{24}$$

then

$$\boldsymbol{x}_1^{\#} = \boldsymbol{s}_1^{\#} + \boldsymbol{x}_{1c}^{\#} = \boldsymbol{s}_1^{\#} + \boldsymbol{y}_1 + \boldsymbol{x}_{1d}^{\#} \tag{25}$$

Simple computations yield that

$$\begin{aligned}\dot{\boldsymbol{s}}_0 = \dot{\boldsymbol{x}}_0 &= \boldsymbol{f}_0 + \boldsymbol{g}_0\boldsymbol{x}_1^{\#} + \boldsymbol{d}_0 \\ &= \boldsymbol{g}_0\left(\boldsymbol{s}_1^{\#} + \boldsymbol{y}_1\right) - \mu_0\boldsymbol{s}_0 + \boldsymbol{g}_0\boldsymbol{k}_0\boldsymbol{s}_0 + \boldsymbol{d}_0\end{aligned} \tag{26}$$

$$\begin{aligned}\dot{\boldsymbol{s}}_1 &= \dot{\boldsymbol{x}}_1 - \begin{bmatrix} 0 \\ \dot{\boldsymbol{x}}_{1c}^{\#} \end{bmatrix} = \boldsymbol{f}_1 + \boldsymbol{g}_1\boldsymbol{x}_2 + \boldsymbol{d}_1 - \begin{bmatrix} 0 \\ \dot{\boldsymbol{x}}_{1c}^{\#} \end{bmatrix} \\ &= -\boldsymbol{k}_1\boldsymbol{s}_1 - \mu_1\boldsymbol{s}_1 + \boldsymbol{g}_1(\boldsymbol{s}_2 + \boldsymbol{y}_2) + \boldsymbol{d}_1\end{aligned} \tag{27}$$

and

$$\dot{\boldsymbol{s}}_2 = \dot{\boldsymbol{x}}_2 - \dot{\boldsymbol{x}}_{2c} = \boldsymbol{f}_2 + \boldsymbol{g}_2\boldsymbol{u} + \boldsymbol{d}_2 - \dot{\boldsymbol{x}}_{2c} = -\boldsymbol{k}_2\boldsymbol{s}_2 - \mu_2\boldsymbol{s}_2 + \boldsymbol{d}_2 \tag{28}$$

Similar to the existing literature on the dynamic surface control approach, for example Ref. [13], etc., here the closed-loop dynamics can be expressed in terms of the dynamic surface vectors, the boundary layer error vectors and the estimate error vectors. That is to say, the closed-loop dynamics can be expressed by Eqs. (17), (18), (19), (26), (27) and (28), or equivalently,

$$\begin{cases} \dot{\boldsymbol{s}}_0 = \boldsymbol{g}_0\left(\boldsymbol{s}_1^{\#} + \boldsymbol{y}_1\right) - \mu_0\boldsymbol{s}_0 + \boldsymbol{g}_0\boldsymbol{k}_0\boldsymbol{s}_0 + \boldsymbol{d}_0 \\ \dot{\boldsymbol{s}}_1 = -\boldsymbol{k}_1\boldsymbol{s}_1 - \mu_1\boldsymbol{s}_1 + \boldsymbol{g}_1(\boldsymbol{s}_2 + \boldsymbol{y}_2) + \boldsymbol{d}_1 \\ \dot{\boldsymbol{s}}_2 = -\boldsymbol{k}_2\boldsymbol{s}_2 - \mu_2\boldsymbol{s}_2 + \boldsymbol{d}_2 \\ \dot{\boldsymbol{y}}_1 = -\boldsymbol{\tau}_1^{-1}\boldsymbol{y}_1 - \dot{\boldsymbol{x}}_{1d}^{\#} \\ \dot{\boldsymbol{y}}_2 = -\boldsymbol{\tau}_2^{-1}\boldsymbol{y}_2 - \dot{\boldsymbol{x}}_{2d} \\ \dot{e}_i = -\lambda_i\left(\boldsymbol{s}_i^{\mathrm{T}}\boldsymbol{s}_i - \sigma_i\mu_i\right) \quad (i = 0, 1, 2) \end{cases} \tag{29}$$

Define the candidate Lyapunov function as

$$E = \frac{1}{2}\sum_{i=0}^{2}\boldsymbol{s}_i^{\mathrm{T}}\boldsymbol{s}_i + \frac{1}{2}\sum_{j=1}^{2}\boldsymbol{y}_j^{\mathrm{T}}\boldsymbol{y}_j + \frac{1}{2}\sum_{i=0}^{2}\frac{1}{\lambda_i}e_i^2 \tag{30}$$

then

$$\dot{E} = \sum_{i=0}^{2}\boldsymbol{s}_i^{\mathrm{T}}\dot{\boldsymbol{s}}_i + \sum_{j=1}^{2}\boldsymbol{y}_j^{\mathrm{T}}\dot{\boldsymbol{y}}_j + \sum_{i=0}^{2}\frac{1}{\lambda_i}e_i\dot{e}_i \tag{31}$$

Direct computations yield that

$$\begin{aligned}\boldsymbol{s}_0^{\mathrm{T}}\dot{\boldsymbol{s}}_0 &= \boldsymbol{s}_0^{\mathrm{T}}\boldsymbol{g}_0\left(\boldsymbol{s}_1^{\#} + \boldsymbol{y}_1\right) - \mu_0\boldsymbol{s}_0^{\mathrm{T}}\boldsymbol{s}_0 + \boldsymbol{s}_0^{\mathrm{T}}\boldsymbol{g}_0\boldsymbol{k}_0\boldsymbol{s}_0 + \boldsymbol{s}_0^{\mathrm{T}}\boldsymbol{d}_0 \\ &\leqslant \boldsymbol{s}_0^{\mathrm{T}}\left(\frac{1}{2}\boldsymbol{g}_0^2 + \boldsymbol{g}_0\boldsymbol{k}_0 + e_0\right)\boldsymbol{s}_0 + \boldsymbol{s}_1^{\mathrm{T}}\boldsymbol{s}_1 + \boldsymbol{y}_1^{\mathrm{T}}\boldsymbol{y}_1 + \frac{1}{4}\rho_0\end{aligned} \tag{32}$$

$$\begin{aligned}\boldsymbol{s}_1^{\mathrm{T}}\dot{\boldsymbol{s}}_1 &= -\boldsymbol{s}_1^{\mathrm{T}}\boldsymbol{k}_1\boldsymbol{s}_1 - \mu_1\boldsymbol{s}_1^{\mathrm{T}}\boldsymbol{s}_1 + \boldsymbol{s}_1^{\mathrm{T}}\boldsymbol{g}_1(\boldsymbol{s}_2 + \boldsymbol{y}_2) + \boldsymbol{s}_1^{\mathrm{T}}\boldsymbol{d}_1 \\ &\leqslant -\boldsymbol{s}_1^{\mathrm{T}}(\boldsymbol{k}_1 + \mu_1)\boldsymbol{s}_1 + \|\boldsymbol{s}_1\|\|\boldsymbol{g}_1\|\|\boldsymbol{s}_2 + \boldsymbol{y}_2\| + \|\boldsymbol{s}_1\|\rho_1 \\ &\leqslant \boldsymbol{s}_1^{\mathrm{T}}\left(e_1 + \frac{1}{2}\|\boldsymbol{g}_1\|^2 - \boldsymbol{k}_1\right)\boldsymbol{s}_1 + \|\boldsymbol{s}_2\|^2 + \|\boldsymbol{y}_2\|^2 + \frac{1}{4}\rho_1\end{aligned} \tag{33}$$

$$\begin{aligned}\boldsymbol{s}_2^{\mathrm{T}}\dot{\boldsymbol{s}}_2 &= -\boldsymbol{s}_2^{\mathrm{T}}\boldsymbol{k}_2\boldsymbol{s}_2 - \mu_2\boldsymbol{s}_2^{\mathrm{T}}\boldsymbol{s}_2 + \boldsymbol{s}_2^{\mathrm{T}}\boldsymbol{d}_2 \\ &\leqslant -\boldsymbol{s}_2^{\mathrm{T}}\boldsymbol{k}_2\boldsymbol{s}_2 - \mu_2\boldsymbol{s}_2^{\mathrm{T}}\boldsymbol{s}_2 + \|\boldsymbol{s}_2\|\rho_2 \\ &\leqslant -\boldsymbol{s}_2^{\mathrm{T}}\boldsymbol{k}_2\boldsymbol{s}_2 + e_2\|\boldsymbol{s}_2\|^2 + \frac{1}{4}\rho_2\end{aligned} \tag{34}$$

$$\boldsymbol{y}_1^{\mathrm{T}}\dot{\boldsymbol{y}}_1 = -\boldsymbol{y}_1^{\mathrm{T}}\boldsymbol{\tau}_1^{-1}\boldsymbol{y}_1 - \boldsymbol{y}_1^{\mathrm{T}}\dot{\boldsymbol{x}}_{1d}^{\#} \leqslant \boldsymbol{y}_1^{\mathrm{T}}\left(\frac{1}{2}\|\dot{\boldsymbol{x}}_{1d}^{\#}\|^2 - \boldsymbol{\tau}_1^{-1}\right)\boldsymbol{y}_1 + \frac{1}{2} \tag{35}$$

$$\boldsymbol{y}_2^{\mathrm{T}}\dot{\boldsymbol{y}}_2 = -\boldsymbol{y}_2^{\mathrm{T}}\boldsymbol{\tau}_2^{-1}\boldsymbol{y}_2 - \boldsymbol{y}_2^{\mathrm{T}}\dot{\boldsymbol{x}}_{2d} \leqslant \boldsymbol{y}_2^{\mathrm{T}}\left(\frac{1}{2}\|\dot{\boldsymbol{x}}_{2d}\|^2 - \boldsymbol{\tau}_2^{-1}\right)\boldsymbol{y}_2 + \frac{1}{2} \tag{36}$$

and

$$\frac{1}{\lambda_i}e_i\dot{e}_i = -e_i\boldsymbol{s}_i^{\mathrm{T}}\boldsymbol{s}_i + \sigma_i e_i \mu_i = -e_i\boldsymbol{s}_i^{\mathrm{T}}\boldsymbol{s}_i + \frac{1}{2}\sigma_i\rho_i^2 - \frac{1}{2}\sigma_i e_i^2 \quad (i = 0, 1, 2) \tag{37}$$

Then we have

$$\begin{aligned}\dot{E} \leqslant\ & \boldsymbol{s}_0^{\mathrm{T}}\left(\frac{1}{2}\boldsymbol{g}_0^2 + \boldsymbol{g}_0\boldsymbol{k}_0\right)\boldsymbol{s}_0 + \boldsymbol{s}_1^{\mathrm{T}}\left(\frac{1}{2}\|\boldsymbol{g}_1\|^2 - \boldsymbol{k}_1 + \boldsymbol{I}_3\right)\boldsymbol{s}_1 \\ & + \boldsymbol{s}_2^{\mathrm{T}}(\boldsymbol{I}_3 - \boldsymbol{k}_2)\boldsymbol{s}_2 + \boldsymbol{y}_1^{\mathrm{T}}\left(\boldsymbol{I}_2 + \frac{1}{2}\left\|\dot{\boldsymbol{x}}_{1\mathrm{c}}^{\#}\right\|^2 - \boldsymbol{\tau}_1^{-1}\right)\boldsymbol{y}_1 \\ & + \boldsymbol{y}_2^{\mathrm{T}}\left(\boldsymbol{I}_3 + \frac{1}{2}\|\dot{\boldsymbol{x}}_{2\mathrm{c}}\|^2 - \boldsymbol{\tau}_2^{-1}\right)\boldsymbol{y}_2 - \frac{1}{2}\sum_{i=0}^{2}\sigma_i e_i^2 + C\end{aligned} \tag{38}$$

where

$$C = \sum_{i=0}^{2}\left(\frac{1}{2}\sigma_i\rho_i^2 + \frac{1}{4}\rho_i\right) + 1 \tag{39}$$

By some tedious but straightforward calculations (please see Appendix A), we have

$$\|\boldsymbol{g}_1\| \leqslant \eta_0(\boldsymbol{s}_0, \boldsymbol{s}_1, \boldsymbol{y}_1, e_0, \boldsymbol{k}_0, \vartheta) \tag{40}$$

$$\left\|\dot{\boldsymbol{x}}_{1\mathrm{d}}^{\#}\right\| \leqslant \eta_1(\boldsymbol{s}_0, \boldsymbol{s}_1, \boldsymbol{y}_1, e_0, \boldsymbol{k}_0, \lambda_0, \sigma_0) \tag{41}$$

$$\|\dot{\boldsymbol{x}}_{2\mathrm{d}}\| \leqslant \eta_2(\boldsymbol{s}_0, \boldsymbol{s}_1, \boldsymbol{s}_2, \boldsymbol{y}_1, \boldsymbol{y}_2, e_0, e_1, \boldsymbol{k}_0, \boldsymbol{k}_1, \boldsymbol{\tau}_1, \lambda_0, \sigma_0, \lambda_1, \sigma_1, \vartheta) \tag{42}$$

where η_0, η_1 and η_2 are both nonnegative continuous functions. Given any $p > 0$, the set

$$B_1 = \left\{\begin{bmatrix}\boldsymbol{s}_0^{\mathrm{T}} & \boldsymbol{s}_1^{\mathrm{T}} & \boldsymbol{s}_2^{\mathrm{T}} & \boldsymbol{y}_1^{\mathrm{T}} & \boldsymbol{y}_2^{\mathrm{T}} & e_0 & e_1 & e_2\end{bmatrix}^{\mathrm{T}} : E \leqslant p\right\}$$

is compact since E is a continuous function with respect to $\begin{bmatrix}\boldsymbol{s}_0^{\mathrm{T}} & \boldsymbol{s}_1^{\mathrm{T}} & \boldsymbol{s}_2^{\mathrm{T}} & \boldsymbol{y}_1^{\mathrm{T}} & \boldsymbol{y}_2^{\mathrm{T}} & e_0 & e_1 & e_2\end{bmatrix}^{\mathrm{T}}$. Hence, the set $B_1 \times B_2$ (the direct product[21] of B_1 and B_2) is also compact. Therefore, η_0, η_1 and η_2 have maximums, say M_0, M_1 and M_2 on $B_1 \times B_2$. As a result, we have

$$\begin{aligned}\dot{E} \leqslant\ & \boldsymbol{s}_0^{\mathrm{T}}\left(\frac{1}{2}\boldsymbol{g}_0^2 + \boldsymbol{g}_0\boldsymbol{k}_0\right)\boldsymbol{s}_0 + \boldsymbol{s}_1^{\mathrm{T}}\left(\frac{1}{2}M_0^2 - \boldsymbol{k}_1 + \boldsymbol{I}_3\right)\boldsymbol{s}_1 + \boldsymbol{s}_2^{\mathrm{T}}(\boldsymbol{I}_3 \\ & - \boldsymbol{k}_2)\boldsymbol{s}_2 + \boldsymbol{y}_1^{\mathrm{T}}\left(\boldsymbol{I}_2 + \frac{1}{2}M_1^2 - \boldsymbol{\tau}_1^{-1}\right)\boldsymbol{y}_1 \\ & + \boldsymbol{y}_2^{\mathrm{T}}\left(\boldsymbol{I}_3 + \frac{1}{2}M_2^2 - \boldsymbol{\tau}_2^{-1}\right)\boldsymbol{y}_2 - \frac{1}{2}\sum_{i=0}^{2}\sigma_i e_i^2 + C\end{aligned} \tag{43}$$

If the design parameters are selected such that

$$\begin{cases}\frac{1}{2}\boldsymbol{g}_0^2 + \boldsymbol{g}_0\boldsymbol{k}_0 \leqslant -\frac{1}{2}\kappa\boldsymbol{I}_2 \\ \frac{1}{2}M_0^2 - \boldsymbol{k}_1 + \boldsymbol{I}_3 \leqslant -\frac{1}{2}\kappa\boldsymbol{I}_3 \\ \boldsymbol{I}_3 - \boldsymbol{k}_2 \leqslant -\frac{1}{2}\kappa\boldsymbol{I}_3 \\ \boldsymbol{I}_2 + \frac{1}{2}M_1^2 - \boldsymbol{\tau}_1^{-1} \leqslant -\frac{1}{2}\kappa\boldsymbol{I}_2 \\ \boldsymbol{I}_3 + \frac{1}{2}M_2^2 - \boldsymbol{\tau}_2^{-1} \leqslant -\frac{1}{2}\kappa\boldsymbol{I}_3 \\ \lambda_i\sigma_i \geqslant \kappa\end{cases} \tag{44}$$

where κ is a positive real number, then we have

$$\dot{E} \leqslant -\kappa E + C \tag{45}$$

If $E = p$ and $\kappa > C/p$, then $\mathrm{d}E/\mathrm{d}t \leqslant 0$. This implies that $E(t) < p$ for all $t > 0$ if $E(0) \leqslant p$. By comparison principle,[22] it is easy from Eq. (44) to obtain that

$$0 \leqslant E(t) \leqslant \frac{C}{\kappa} + \left(E(0) - \frac{C}{\kappa}\right)\exp(-\kappa t) \tag{46}$$

Therefore, $\boldsymbol{s}_0$, $\boldsymbol{s}_1$, $\boldsymbol{s}_2$, $\boldsymbol{y}_1$, $\boldsymbol{y}_2$, e_0, e_1 and e_2, are all uniformly ultimately bounded. Furthermore, $\boldsymbol{x}_0$, $\boldsymbol{x}_1$ and $\boldsymbol{x}_2$ are all uniformly ultimately bounded. In addition, it is easy to see that for given σ_i, C is a constant independent of κ, so C/κ can be made arbitrarily small by choosing κ big enough. This implies that $\boldsymbol{s}_0$ and $\boldsymbol{s}_1$ can be made arbitrarily small ultimately. Hence, x_{01}, x_{02} and x_{11} can be made arbitrarily small ultimately.

To sum up, we have the following theorem.

Theorem 1. *For the uncertain nonlinear system (10) satisfying Assumptions 1-3, the robust adaptive dynamic surface control algorithm (11) with appropriate design parameters can keep all the states of the closed-loop system bounded and ultimately drive the partial states x_{01}, x_{02} and x_{11} into a neighborhood of zero whose size can be reduced by increasing the design parameters k_{ij} and $\lambda_i\sigma_j$ and reducing the design parameters τ_{ij} at the same time.*

Remark 3. The design parameters include k_0, k_1, k_2, τ_1, τ_2, λ_0, λ_1, λ_2, σ_0, σ_1 and σ_2. M_0 depends only on k_0. M_1 depends only on k_0, λ_0 and σ_0. M_2 depends only on k_0, k_1, τ_1, λ_0, λ_1, σ_0 and σ_1. Hence, according to Eq. (44), the design parameters λ_0, λ_1, λ_2, σ_0, σ_1, σ_2 and k_2 can be selected easily; but for the design parameters k_0, k_1, τ_1 and τ_2, k_0 should be selected firstly, then one can select k_1 and τ_1, and further, one can select τ_2.

Remark 4. Similar to the existing literature on the dynamic surface control method (e.g., Refs. [12,13], etc.), Theorem 1 shows the existence of the control algorithm to ensure the stability of the closed-loop system but does not provide a quantitative criterion on how to select the design parameters. In fact, it is very difficult to give such a criterion. By far, the design parameters can only be selected by trial and error.

Remark 5. Theoretically speaking, the bigger the design parameters k_{ij} and $\lambda_i\sigma_j$ are, and meanwhile the smaller the design parameters τ_{ij} are, the smaller the ultimate bounds of the states x_{01}, x_{02} and x_{11} (i.e., $\dot{\eta}$, $\dot{\varepsilon}$ and γ) will be; as a result, the smaller the miss distance will be. However, a large amount of simulation experiments show that it may lead to unsatisfactory or even unacceptable transient performance of the closed-loop system if the dynamic surface gains k_{ij} are selected too big and the filter time constants τ_{ij} are selected too small. For example, the transient values of the key states α and β may become too big to satisfy the practical requirements. Therefore, the design parameters should be adjusted by trading off between the transient performance and the precision of the regulation.

4. Numerical simulations

In this section, the effectiveness of the proposed integrated missile guidance and autopilot algorithm based on the adaptive dynamic surface control approach is verified by the 6DOF nonlinear numerical simulations.

It is noted that system (10) is only used for the integrated guidance and autopilot design, but not for the 6DOF nonlinear numerical simulations. For the 6DOF nonlinear numerical simulations, the original nonlinear motion model of the missile given in Ref. [17] is adopted, where the aerodynamic forces and moments are given as follows:

$$\begin{cases} X = qS\left(c_{x0} + c_x^{\alpha}|\alpha| + c_x^{\beta}|\beta| + c_x^{\alpha\beta}|\alpha\beta| + c_x^{\delta_x}|\delta_x| + c_x^{\delta_y}|\delta_y| + c_x^{\delta_z}|\delta_z|\right) \\ Y = qS\left(c_y^{\alpha}\alpha + c_y^{\beta}\beta + c_y^{\delta_z}\delta_z\right) \\ Z = qS\left(c_z^{\alpha}\alpha + c_z^{\beta}\beta + c_z^{\delta_y}\delta_y\right) \\ M_x = qSL\left(m_x^{\alpha}\alpha + m_x^{\beta}\beta + m_x^{\delta_x}\delta_x\right) \\ M_y = qSL\left(m_y^{\beta}\beta + m_y^{\delta_y}\delta_y\right) \\ M_z = qSL\left(m_z^{\alpha}\alpha + m_z^{\delta_z}\delta_z\right) \end{cases} \tag{47}$$

In the inertial coordinate system, the motion model of the target is described by

$$\begin{cases} \dot{\boldsymbol{x}}_{\mathrm{t}} = \boldsymbol{V}_{\mathrm{t}} \\ \dot{\boldsymbol{V}}_{\mathrm{t}} = \boldsymbol{a}_{\mathrm{t}} \end{cases} \tag{48}$$

where $\boldsymbol{x}_{\mathrm{t}} = [x_{\mathrm{t}} \quad y_{\mathrm{t}} \quad z_{\mathrm{t}}]^{\mathrm{T}}$, $\boldsymbol{V}_{\mathrm{t}} = [V_{\mathrm{t}x} \quad V_{\mathrm{t}y} \quad V_{\mathrm{t}z}]^{\mathrm{T}}$ and $\boldsymbol{a}_{\mathrm{t}} = [a_{\mathrm{t}x} \quad a_{\mathrm{t}y} \quad a_{\mathrm{t}z}]^{\mathrm{T}}$ are, respectively, the position, velocity and acceleration vectors of the target.

Define $\boldsymbol{x}_{\mathrm{m}} = [x_{\mathrm{m}}\ y_{\mathrm{m}}\ z_{\mathrm{m}}]^{\mathrm{T}}$ to be the position vector of the missile in the inertial coordinate system, then the states R, r, ε and η are calculated by

$$\begin{cases} R = \sqrt{(x_{\mathrm{t}} - x_{\mathrm{m}})^2 + (y_{\mathrm{t}} - y_{\mathrm{m}})^2 + (z_{\mathrm{t}} - z_{\mathrm{m}})^2} \\ r = \sqrt{(x_{\mathrm{t}} - x_{\mathrm{m}})^2 + (z_{\mathrm{t}} - z_{\mathrm{m}})^2} \\ \varepsilon = \arctan\left(\frac{y_{\mathrm{t}} - y_{\mathrm{m}}}{r}\right) \\ \eta = -\arctan\left(\frac{z_{\mathrm{t}} - z_{\mathrm{m}}}{x_{\mathrm{t}} - x_{\mathrm{m}}}\right) \end{cases} \tag{49}$$

The initial position, the initial velocity and the acceleration vectors of the target are, respectively, set as

$$\begin{cases} \boldsymbol{x}_{\mathrm{t}}(0) = [3000 \quad 0 \quad 300]^{\mathrm{T}}\mathrm{m} \\ \boldsymbol{V}_{\mathrm{t}}(0) = [30 \quad 0 \quad 40]^{\mathrm{T}}\mathrm{m/s} \\ \boldsymbol{a}_{\mathrm{t}} = [4 \quad 0 \quad 3]^{\mathrm{T}}\mathrm{m/s^2} \end{cases}$$

For the missile, the initial position coordinate vector in the inertial coordinate system is set as

$$\boldsymbol{x}_{\mathrm{m}}(0) = [0 \quad 3000 \quad 0]^{\mathrm{T}}\mathrm{m}$$

The velocity, the pitch, yaw and roll angles, the flight path and heading angles, the pitch, yaw and roll rates at initial time are, respectively, set as

$$\begin{array}{lll} V(0) = 200\ \mathrm{m/s}, & \vartheta(0) = 0.02\ \mathrm{rad}, & \psi(0) = 0.01\ \mathrm{rad} \\ \gamma(0) = 0\ \mathrm{rad}, & \theta(0) = 0.01\ \mathrm{rad}, & \psi_V(0) = -0.01\ \mathrm{rad} \\ \omega_x(0) = 0.1\ \mathrm{rad/s}, & \omega_y(0) = 0.1\ \mathrm{rad/s}, & \omega_z(0) = 0.1\ \mathrm{rad/s} \end{array}$$

In order to test the performance of the proposed integrated guidance and autopilot algorithm when there are uncertainties in the missile-related parameters, two hundred times of Monte Carlo simulation experiments are done.

Use $N(0,1)$ to generate a number from a normal distribution with mean 0 and standard deviation 1. Based on this, we define N_{T} as

$$N_{\mathrm{T}} = \begin{cases} -1 & \frac{1}{3}N(0,1) < -1 \\ \frac{1}{3}N(0,1) & -1 < \frac{1}{3}N(0,1) < 1 \\ 1 & \frac{1}{3}N(0,1) > 1 \end{cases} \tag{50}$$

Remark 6. N_{T} is used to generate a random number in the interval $[-1,\ 1]$. It is noted that in the sequel, for each occurrence of N_{T}, it almost always denotes a different number.

With the help of N_{T}, the missile-related parameters used in the Monte Carlo simulation experiments are given in Table 1.

Remark 7. For the formulas of the parameters' values in Table 1, the numbers before the brackets denote the nominal values of these parameters. These nominal values are used in the integrated guidance and autopilot algorithm.

The main requirements for the present design are as follows:

(1) the miss distance is no greater than 0.1 m.
(2) the angles of attack and sideslip are both no greater than 8°.
(3) the change of the roll angle is no greater than 1°.
(4) the states of the missile are bounded.
(5) the above four requirements are satisfied when considering the uncertainties of missile-related parameters.

Table 1 Missile-related parameters.

Name	Value	Name	Value	Name	Value
m	$1200(1 + 0.1N_{\mathrm{T}})$	m_y^{β}	$-27.31(1 + 0.2N_{\mathrm{T}})$	$c_x^{\delta_x}$	$0.05(1 + 0.2N_{\mathrm{T}})$
P	$3500(1 + 0.1N_{\mathrm{T}})$	$m_y^{\delta_y}$	$-26.57(1 + 0.2N_{\mathrm{T}})$	$c_x^{\delta_y}$	$0.07(1 + 0.2N_{\mathrm{T}})$
J_x	$100(1 + 0.1N_{\mathrm{T}})$	$m_x^{\delta_x}$	$2.12(1 + 0.2N_{\mathrm{T}})$	$c_x^{\delta_z}$	$0.06(1 + 0.2N_{\mathrm{T}})$
J_y	$5700(1 + 0.1N_{\mathrm{T}})$	m_x^{α}	$0.46(1 + 0.2N_{\mathrm{T}})$	c_y^{α}	$57.16(1 + 0.2N_{\mathrm{T}})$
J_z	$5600(1 + 0.1N_{\mathrm{T}})$	m_x^{β}	$-0.37(1 + 0.2N_{\mathrm{T}})$	$c_y^{\delta_z}$	$5.74(1 + 0.2N_{\mathrm{T}})$
S	$0.42(1 + 0.1N_{\mathrm{T}})$	c_{x0}	$0.32(1 + 0.2N_{\mathrm{T}})$	c_y^{β}	$-0.08(1 + 0.2N_{\mathrm{T}})$
L	$0.68(1 + 0.1N_{\mathrm{T}})$	c_x^{α}	$0.21(1 + 0.2N_{\mathrm{T}})$	c_z^{β}	$-56.31(1 + 0.2N_{\mathrm{T}})$
m_z^{α}	$-28.16(1 + 0.2N_{\mathrm{T}})$	c_x^{β}	$0.19(1 + 0.2N_{\mathrm{T}})$	$c_z^{\delta_y}$	$-5.62(1 + 0.2N_{\mathrm{T}})$
$m_z^{\delta_z}$	$-27.92(1 + 0.2N_{\mathrm{T}})$	$c_x^{\alpha\beta}$	$25.38(1 + 0.2N_{\mathrm{T}})$	c_z^{α}	$0.09(1 + 0.2N_{\mathrm{T}})$

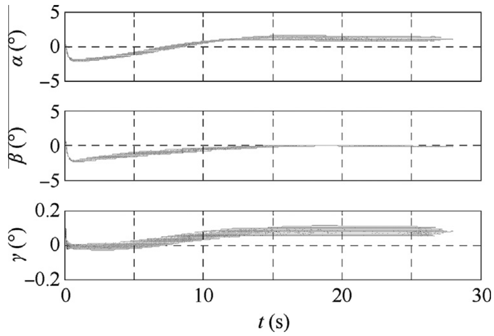

Fig. 2 Curves of the angles α, β and γ.

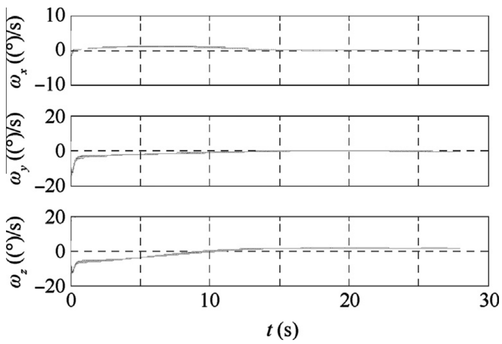

Fig. 3 Curves of angular rates ω_x, ω_y and ω_z.

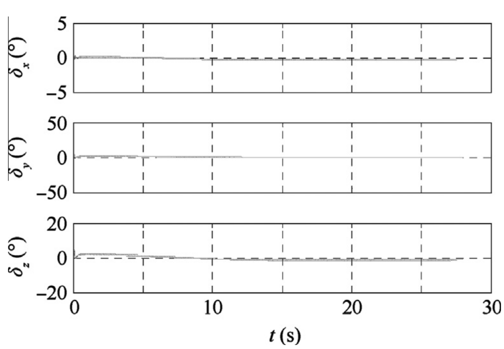

Fig. 4 Curves of the fin deflections δ_x, δ_y and δ_z.

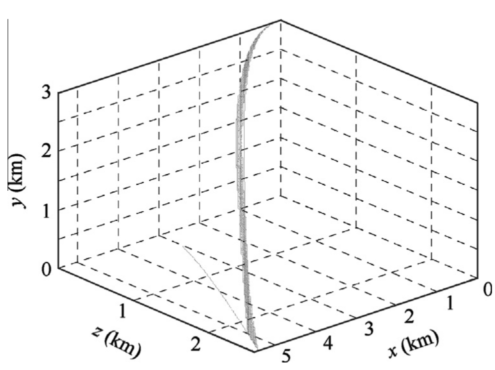

Fig. 5 Trajectories of the missile and the target (the trajectory of the target lies on the x–z plane).

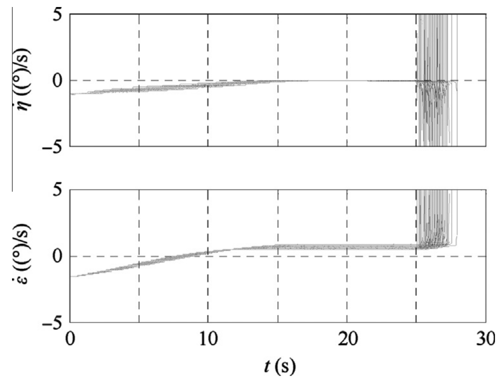

Fig. 6 Curves of the derivatives of η and ε.

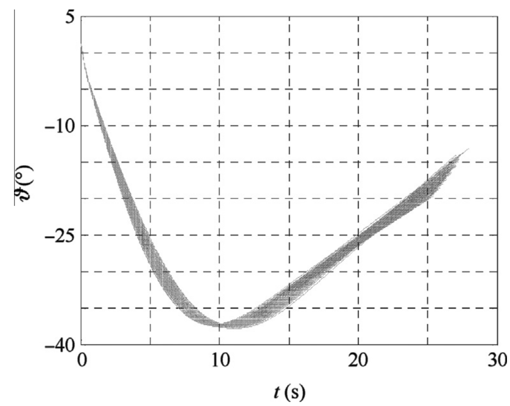

Fig. 7 Curves of pitch angle ϑ.

The results of the Monte Carlo simulation experiments are shown in Figs. 2–7. The mean miss distance is 0.04 m with standard deviation 0.02 m. This means that the missile can intercept the maneuvering targets with very small miss distance. The third subfigure of Fig. 2 shows that the roll angle $|\gamma| < 0.2°$, that is, the change of the roll angle can be kept near zero throughout the engagement. Figs. 2, 3 and 6 show that the states of the missile are bounded. In addition, in the Monte Carlo simulation experiments, the uncertainties of the missile-related parameters have been fully considered, hence it is reasonable to say that the proposed integrated guidance and autopilot is robust with respect to the inevitable uncertainties existing in the missile dynamics. These imply that the design objectives of the integrated guidance and autopilot system are achieved.

Remark 8. It is noted that in Fig. 6, the derivatives of η and ε are diverging. This is consistent with the reality since the missile–target range is converging to zero finally. But this problem is insignificant since the integrated guidance and control system will stop working when these two variables become big enough.

Remark 9. From Figs. 2 and 7, we can see that $|\alpha| < 5°$, $|\beta| < 5°$ and $\vartheta > -40°$. It is easy to check that

$$\det(\boldsymbol{g}_1(\vartheta, \boldsymbol{x}_1)) > 0$$

always holds. Hence, $g_1(\vartheta, x_1)$ is always invertible.

Remark 10. It should be pointed out that it is assumed in this paper that the angles of attack and sideslip are available for the integrated guidance and autopilot algorithm design. Although it is generally difficult to measure these angles directly in practice, there already exist some effective methods to estimate them. The interested readers can refer to Ref. [23] and the references therein for detail.

5. Conclusions

In this paper, a novel fully integrated guidance and autopilot design scheme is proposed for homing missiles. The couplings between the guidance system and the autopilot system and those between different channels (i.e., the roll, the yaw and the pitch channels) of the missile dynamics are fully and explicitly considered in the design procedure. The proposed integrated guidance and autopilot algorithm is based on a new adaptive block dynamic surface control method. It is simple and analytic, and can avoid complicated computations compared to the existing ones. Also, the effectiveness of the proposed integrated guidance and autopilot algorithm is demonstrated by the 6DOF nonlinear numerical simulation results.

Acknowledgements

The authors are grateful to the anonymous reviewers for their critical and constructive review of the manuscript. This study was co-supported by the Fundamental Research Funds for the Central Universities (No. HIT. NSRIF. 2013039) and the National Natural Science Foundation of China (Nos. 61203125 and 61021002).

Appendix A.

First of all, define $\boldsymbol{\eta}_*(\cdot)$ and $\eta_*(\cdot)$ to be continuous functions indexed by "*".

According to Eq. (21),

$$\boldsymbol{x}_0 = \boldsymbol{s}_0 \tag{A.1}$$

then from Eq. (11) and Assumptions 1 and 2, we have

$$\boldsymbol{x}_{1d}^{\#} = \boldsymbol{\eta}_{x1d\#}(\boldsymbol{s}_0, e_0, \boldsymbol{k}_0) \tag{A.2}$$

Then from Eqs. (22) and (25), one can obtain

$$\boldsymbol{x}_1 = \boldsymbol{\eta}_{x1}(\boldsymbol{s}_0, \boldsymbol{s}_1, \boldsymbol{y}_1, e_0, \boldsymbol{k}_0) \tag{A.3}$$

$$\boldsymbol{x}_1^{\#} = \boldsymbol{\eta}_{x1\#}(\boldsymbol{s}_0, \boldsymbol{s}_1, \boldsymbol{y}_1, e_0, \boldsymbol{k}_0) \tag{A.4}$$

Combining Eq. (13) with Eq. (15), it can be obtained that

$$\dot{\boldsymbol{x}}_{1c}^{\#} = -\boldsymbol{\tau}_1^{-1}\boldsymbol{y}_1 \tag{A.5}$$

From Eq. (29) and Assumptions 1 and 2, we have

$$\|\dot{\boldsymbol{s}}_0\| \leqslant \eta_{s_0}(\boldsymbol{s}_0, \boldsymbol{s}_1, \boldsymbol{y}_1, e_0, \boldsymbol{k}_0) \tag{A.6}$$

and

$$\|\dot{\boldsymbol{s}}_1\| \leqslant \eta_{s_1}(\boldsymbol{s}_0, \boldsymbol{s}_1, \boldsymbol{s}_2, \boldsymbol{y}_1, \boldsymbol{y}_2, e_0, e_1, \boldsymbol{k}_0, \boldsymbol{k}_1, \vartheta) \tag{A.7}$$

Hence, from Eqs. (A.1) and (A.6), we can see

$$\|\dot{\boldsymbol{x}}_0\| \leqslant \eta_{x_0}(\boldsymbol{s}_0, \boldsymbol{s}_1, \boldsymbol{y}_1, e_0, \boldsymbol{k}_0) \tag{A.8}$$

From Eq. (22), we have

$$\dot{\boldsymbol{x}}_1 = \dot{\boldsymbol{s}}_1 + \left[0 \quad \left(\dot{\boldsymbol{x}}_{1c}^{\#}\right)^{\mathrm{T}}\right]^{\mathrm{T}} \tag{A.9}$$

The combination of Eq. (A.9) with Eqs. (A.5) and (A.7) yields

$$\|\dot{\boldsymbol{x}}_1\| \leqslant \eta_{x_1}(\boldsymbol{s}_0, \boldsymbol{s}_1, \boldsymbol{s}_2, \boldsymbol{y}_1, \boldsymbol{y}_1, e_0, e_1, \boldsymbol{k}_0, \boldsymbol{k}_1, \boldsymbol{\tau}_1, \vartheta) \tag{A.10}$$

From Eqs. (12) and (17), we have

$$\dot{\mu}_i = \lambda_i\left(\boldsymbol{s}_i^{\mathrm{T}}\boldsymbol{s}_i + \sigma_i e_i - \sigma_i \rho_i\right) \tag{A.11}$$

This together with Assumption 1 yields

$$|\dot{\mu}_i| \leqslant \eta_{\mu_i}(\boldsymbol{s}_i, e_i, \lambda_i, \sigma_i) \tag{A.12}$$

From Eq. (11), we have

$$\begin{aligned}\dot{\boldsymbol{x}}_{1d}^{\#} = & -\dot{\boldsymbol{g}}_0^{-1}(t)(\mu_0\boldsymbol{s}_0 + \boldsymbol{f}_0(\boldsymbol{x}_0)) + \boldsymbol{k}_0\dot{\boldsymbol{s}}_0 \\ & - \boldsymbol{g}_0^{-1}(t)\left(\dot{\mu}_0\boldsymbol{s}_0 + \mu_0\dot{\boldsymbol{s}}_0 + \frac{\partial \boldsymbol{f}_0}{\partial \boldsymbol{x}_0}\dot{\boldsymbol{x}}_0\right)\end{aligned} \tag{A.13}$$

Hence, it is easy from Eqs. (A.1), (A.6), (A.8), (A.12) and Assumptions 1–2 to obtain the inequality (41).

Further, we have

$$\|\dot{\boldsymbol{y}}_1\| \leqslant -\boldsymbol{\tau}_1^{-1}\boldsymbol{y}_1 - \dot{\boldsymbol{x}}_{1d}^{\#} \tag{A.14}$$

From (11), (A.3) and (A.5) and Assumption 1, we have

$$\boldsymbol{x}_{2d} = \boldsymbol{\eta}_{x2d}(\boldsymbol{s}_0, \boldsymbol{s}_1, \boldsymbol{y}_1, e_0, e_1, \boldsymbol{k}_0, \boldsymbol{k}_1, \boldsymbol{\tau}_1, \vartheta) \tag{A.15}$$

Then from (23), we have

$$\boldsymbol{x}_2 = \boldsymbol{\eta}_{x_2}(\boldsymbol{s}_0, \boldsymbol{s}_1, \boldsymbol{s}_2, \boldsymbol{y}_1, \boldsymbol{y}_2, e_0, e_1, \boldsymbol{k}_0, \boldsymbol{k}_1, \boldsymbol{\tau}_1, \vartheta) \tag{A.16}$$

Again, from Eqs. (11) and (A.5), we have

$$\begin{aligned}\dot{\boldsymbol{x}}_{2d} = & \left(\frac{\partial \boldsymbol{g}_1^{-1}}{\partial \vartheta}\dot{\vartheta} + \frac{\partial \boldsymbol{g}_1^{-1}}{\partial \boldsymbol{x}_1}\dot{\boldsymbol{x}}_1\right)\left(-\mu_1\boldsymbol{s}_1 - \boldsymbol{k}_1\boldsymbol{s}_1 - \boldsymbol{f}_1(\boldsymbol{x}_1) + \begin{bmatrix} 0 \\ \dot{\boldsymbol{x}}_{1c}^{\#}\end{bmatrix}\right) \\ & + \boldsymbol{g}_1^{-1}(\vartheta, \boldsymbol{x}_1)\left(-\dot{\mu}_1\boldsymbol{s}_1 - \mu_1\dot{\boldsymbol{s}}_1 - \boldsymbol{k}_1\dot{\boldsymbol{s}}_1 - \frac{\partial \boldsymbol{f}_1}{\partial \boldsymbol{x}_1}\dot{\boldsymbol{x}}_1 - \begin{bmatrix} 0 \\ \boldsymbol{\tau}_1^{-1}\dot{\boldsymbol{y}}_1\end{bmatrix}\right)\end{aligned} \tag{A.17}$$

Hence, it is easy from Eqs. (2), (A.5), (A.10), (A.12), (A.14), (A.16) and (A.17) to obtain the inequality (42).

In addition it is easy from Eq. (A.3) to obtain the inequality (40).

References

1. Menon PK, Ohlmeyer EJ. Integrated design of agile missile guidance and autopilot systems. *Control Eng Pract* 2001;**9**(10):1095–106.
2. Palumbo NF, Reardon BE, Blauwkamp RA. Integrated guidance and control for homing missiles. *Johns Hopkins Appl Tech Des* 2004;**25**(2):121–39.
3. Idan M, Shima T, Golan OM. Integrated sliding mode autopilot-guidance for dual-control missiles. *J Guidance Control Dyn* 2007;**30**(4):1081–9.
4. Sharma M, Richards ND. Adaptive, integrated guidance and control for missile interceptors; 2004. Report No.: AIAA-2004-4880.

5. Hou MZ, Duan GR. Integrated guidance and control for homing missiles against ground fixed targets. *Chin J Aeronaut* 2008;**21**(2): 162–8.
6. Duan GR, Hou MZ. Adaptive, integrated guidance and control law design using sliding-mode approach. *Acta Armameentarii* 2010;**31**(2):191–8 [Chinese].
7. Shtessel YB, Tournes CH. Integrated higher-order sliding mode guidance and autopilot for dual control missiles. *J Guidance Control Dyn* 2009;**32**(1):79–94.
8. Vaddi SS, Menon PK, Ohlmeyer EJ. Numerical state-dependent riccati equation approach for missile integrated guidance control. *J Guidance Control Dyn* 2009;**32**(2):699–703.
9. Xin M, Balakrishnan SN, Ohlmeyer EJ. Integrated guidance and control of missiles with θ-D method. *IEEE Trans Control Syst Technol* 2006;**14**(6):981–92.
10. Hou MZ, Duan GR. Adaptive dynamic surface control for integrated missile guidance and autopilot. *Int J Autom Comput* 2011;**8**(1):122–7.
11. Krstic M, Kanellakapoulous I, Kokotovic P. *Nonlinear and adaptive control design*. New York: Wiley Interscience; 1995.
12. Swaroop D, Hedrick JK, Yip PP, Gerdes JC. Dynamic surface control for a class of nonlinear systems. *IEEE Trans Autom Control* 2000;**45**(10):1893–9.
13. Yip PP, Hedrick JK. Adaptive dynamic surface control: a simplified algorithm for adaptive backstepping control of nonlinear systems. *Int J Control* 1998;**71**(5):959–79.
14. Hou MZ, Duan GR. Robust adaptive dynamic surface control of uncertain nonlinear systems. *Int J Control Autom Syst* 2011;**9**(1): 161–8.
15. Zhang YA, Hu YA. *Nonlinear design methods for missile control and guidance*. Beijing: National Defense Industry Press; 2003 [Chinese].
16. Zhu K, Qi NM, Guan YZ, Wang W. A simplified backstepping sliding mode controller based on adaptive control for BTT missiles. In: *Proceedings of the 2009 IEEE International Conference on Mechatronics and Automation; 2009 Aug 9–12*. Changchun, China, Piscataway: IEEE Press; 2009. p. 4583–8.
17. Qian XF, Lin RX, Zhao YN. *Missile flight mechanics*. Beijing: Beijing Institute of Technology Press; 2000 [Chinese].
18. Sun S, Zhou D. Three-dimensional nonlinear guidance law with considering of autopilot dynamics. *J Astronaut* 2009;**30**(3):1052–6 [Chinese].
19. Yang CD, Yang CC. Analytical solution of 3D true proportional navigation. *IEEE Trans Aerosp Electron Syst* 1996;**32**(4):1509–22.
20. Zarchan P. *Tactical and strategic missile guidance*. 2nd ed. Washington, DC: American Institute of Aeronautics and Astronautics Inc; 1994.
21. Apstol TM. *Mathematical analysis*. 2nd ed. White Plains: Addison-Wesley Pub. Co.; 1974.
22. Khalil HK. *Nonlinear systems*. 3rd ed. Upper Saddle River: Prentice Hall; 1996.
23. Colgren R, Frye M, Olson W. A proposed system architecture for estimation of angle-of-attack and sideslip angle; 1999. Report No.: AIAA-1999-4078.

Hou Mingzhe received his Ph.D. degree in navigation, guidance and control from Harbin Institute of Technology in 2011. Currently, he is a lecturer at Center for Control Theory and Guidance Technology, Harbin Institute of Technology. His research interests include nonlinear control and guidance and control of aircraft.

Liang Xiaoling is a Ph.D. student at the Center for Control Theory and Guidance Technology, Harbin Institute of Technology. Her research interests include nonlinear control and control of aircraft.

Duan Guangren received his B.Sc. degree in applied mathematics, and both M.Sc. and Ph.D. degrees in control systems theory. From 1989 to 1991, he was a post-doctoral researcher at Harbin Institute of Technology, where he became a professor of control systems theory in 1991. Prof. Duan visited the University of Hull, UK, and the University of Sheffield, UK from December 1996 to October 1998, and worked at the Queen's University of Belfast, UK from October 1998 to October 2002. Since August 2000, he has been elected Specially Employed Professor at Harbin Institute of Technology sponsored by the Cheung Kong Scholars Program of the Chinese government. He is currently the Director of the Center for Control Systems and Guidance Technology at Harbin Institute of Technology. He is the author and co-author of over 400 publications. Prof. Duan is a Charted Engineer in the UK, a Senior Member of IEEE and a Fellow of IEE. His main research interests include robust control, eigenstructure assignment, descriptor systems, missile autopilot control and magnetic bearing control.